JOURNAL OF MATERIALS SCIENCE 20 (1985) 3897–3905

Fracture toughness and fatigue crack growth of grey cast irons

ERHARD HORNBOGEN
Institut für Werkstoffe, Ruhr-Universität Bochum, D-4630 Bochum, West Germany

The fracture behaviour of alloys with a pearlitic matrix and lamellar and spherulitic graphite has been compared. Fatigue crack growth functions were measured and various critical stress intensities obtained from load–displacement curves. An analysis of microstructure in the uncracked and cracked state served as the base for a discussion of quantitative models for the relation between microstructure and bulk fracture mechanical properties. In addition to volume fraction and shape of graphite, crack branching (and eventually transformation of residual austenite) are required to explain the resistance of grey cast irons against stable and unstable crack growth. It is concluded that the standard methods for the evaluation of fracture mechanical properties are not satisfactory especially for cast irons with lamellar graphite.

1. Introduction

The fracture mechanical properties of grey cast irons have attracted recent attention from two points of view: (1) in the case of sufficient toughness some cast irons will compete successfully with steels. Reliable data on fracture mechanical properties are requested from foundary- and design-engineers: (2) grey cast irons may serve as model materials because of their microstructure consisting of a metallic (steel-like) matrix with graphite which provides quasi-holes of different size, shape, and volume fraction.

An attempt to make a quantitative correlation between this level of microstructure and fracture toughness has been made using the priniciple of "effective stress intensity" [1, 2]. The model implies the calculation of an average internal stress caused by graphite particles with a volume fraction, f_g, length, l, and radius of curvature, ϱ. This additional stress raises that due to the external load in the graphite-free matrix. As a consequence the fracture toughness of the graphite-free matrix, K_{Icm}, is lowered to $K_{Ic} < K_{Icm}$:

$$\frac{K_{Im}}{K_I} = \frac{K_{Ic}}{K_{Icm}} \quad (1)$$

$$K_{Ic} = \frac{K_{Icm}}{f_m + f_g C[1 + 2(l/\varrho)^2]} \quad (2)$$

This relation uses a rather rough approximation for the description of the microstructure of the matrix. Its volume fraction is $f_m = 1 - f_g$. The statistical factor $C \approx 0.5$ considers the distribution of graphite particles. Details of the matrix microstructure such as pro-eutectic dendrites or ferrites seams are not considered. Nevertheless, reasonable predictions can be made for the effect of the shape of graphite on fracture toughness (Fig. 1) [3].

Systematic work on fracture mechanics of cast iron began after 1970 [4–7]. A summary of many results can be found in [7]. In addition, studies on the effect of wall thickness and solidification conditions [8], and of heat treatments [9, 10] have provided substantial information on fracture properties of grey cast iron. The difference in morphology of graphite and of fracture toughness between iron with lamellar and spheroidal graphite explains other important properties such as the superior resistance to abrasive wear of globular irons [11].

It is not surprising that some discrepancies

0022–2461/85 $03.00 + .12

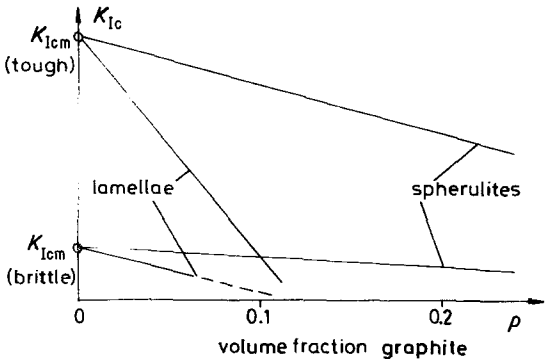

Figure 1 Schematic illustration of the effect of graphite inclusions on fracture toughness of tough (ferrite, pearlite, bainite, austenite) or brittle (martensite) matrix.

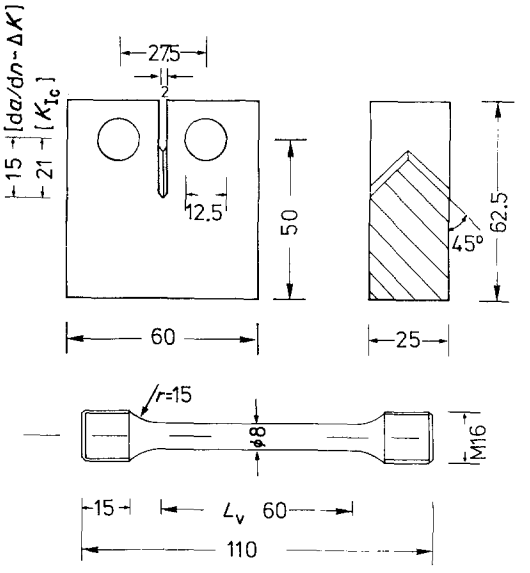

Figure 2 Dimensions of specimens which were used for obtaining mechanical properties.

exist in the fracture mechanical data from the earlier work [6, 7]. This may be due to either scatter in the composition or microstructure of the cast alloys. On the other hand, there exists a variety of methods for the evaluation of the force–displacement curves and for the production of precracks. It may be disputed whether it is reasonable to adhere to the ASTM-Standards for lamellar cast iron [12]. Some authors applied, for example, first pop-in, 95% secant, maximum force for evaluation of critical K-values. The amplitudes, ΔK, used for the production of the pre-crack seem to differ in some of the older investigations. One author evidently designates the maximum amplitude ΔK_m in the fatigue test as K_{Ic} [6]*. The structure of the lamellar cast iron provides additional difficulties with non-linear elasticity, caused by micro-cracks in and at graphite particles in addition to plasticity at the crack tip and at the edges of the graphite lamellae.

J-integral measurements [12b] and J–R curve evaluations [12c] may be considered. It should be carefully distinguished between non-linear elastic and plastic deformation. It is doubtful whether this will provide much additional physical insight into the fracture mechanisms, or more reliable data for dimensioning in design. The careful evaluation of force–displacement curves and their correlation with observed micromechanisms was used in this investigation.

The investigation was conducted with standard grey cast irons with lamellar and spherulitic graphite from different origin, with well documented microstructure and tensile properties. The purpose of the work was two-fold: to obtain reliable data on fracture mechanical properties of the materials which are of great practical importance, and to discuss different ways of their evalution based on the microstructural origin.

2. Materials and experimental procedure

The materials were obtained in the form of as-cast bars of 30 to 35 mm diameter. Chemical composition and microstructure are given in Table I. Two types of specimens were produced for tensile tests, and measurements of fatigue crack growth and fracture toughness (Fig. 2). Special care was taken for the registration of the force–displacement curves. The accuracy for the measurement of the crack displacement was 10^{-1} mm. In some of the static tests the force was reduced and cycled at high amplitudes before final fracture, in order to disclose non-linear elastic behaviour and changes in elastic modulus. The production of the pre-crack was done according to the ASTM Standard at displacements of 10^{-9} m per cycle. In addition, the effect of higher amplitudes of stress intensity up to the end of the da/dN curves was investigated in respect to the consequent static crack propagation.

*The original work presents the same measurements with correct designations (see Fig. 39 in [5]).

TABLE I Chemical composition (wt %) of the alloys

Alloy		C	Mn	Si	P	S	Cu	Ni
1	GG 30 S	3.26	0.67	1.72	0.05	0.01	1.04	–
2	GG 30 T	3.27	0.81	1.59	0.07	0.04	0.35	–
3	GGG 70 T	3.70	0.49	1.87	0.02	0.005	0.30	–
4	GGG 80 S	3.40	0.14	1.84	0.04	0.005	0.74	0.86

All fatigue crack growth curves were obtained with 5 Hz. Special care was required in the determination of the threshold ΔK_{th}. It was defined as the ΔK value at which a crack grew less than 10^{-9} m per cycle. 10^8 cycles were required for one measurement in this range of ΔK (Fig. 3b). Additional difficulties arose from branching and satellite formation near the crack tip.

Light microscopy (LM) and scanning electron microscopy were applied in uncracked, partially and completely cracked specimens. Special attention was paid to direct investigations of the reaction zone ahead of the crack. For such observations a wedge was impressed into the notch of a CT-specimen, while being investigated in a light microscope.

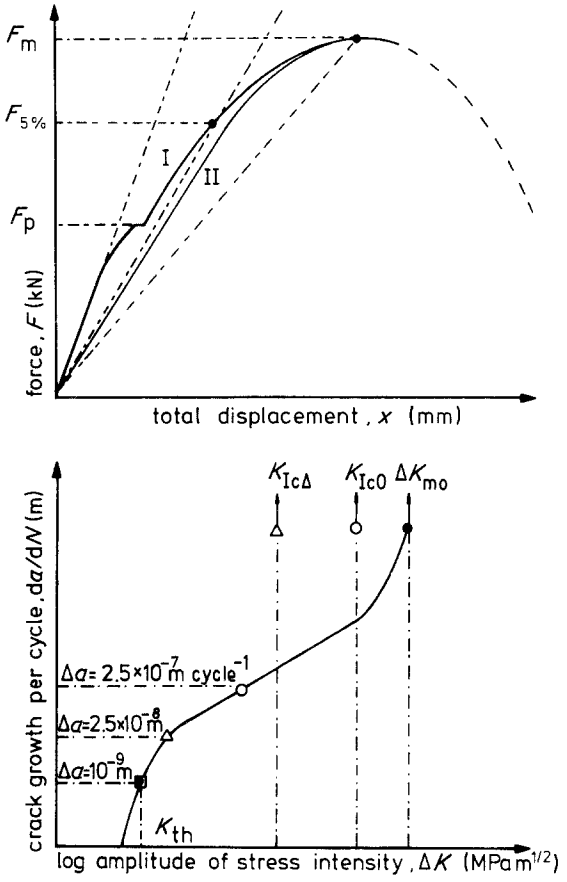

Figure 3 (a) Evaluation of force–displacement curves (pop-in, p; 5% secant, 5%; maximum load, m). (b) Fatigue crack growth, da/dN, and various critical stress intensities, K_c, measured with precracks produced by different displacement amplitudes, Δa_i. Schematic drawing.

3. Experimental results

The microstructures of all materials show a pearlitic matrix with differently shaped graphite (Fig. 4). The data obtained by quantitative metallography are given in Table II. These micrographs should be compared with Fig. 5 in which the interaction with a moving crack can be recognized. The cracks pass through the graphite phase for all loading conditions. There is a tendency for interlamellar crack propagation in the pearlitic matrix for low amplitudes of stress intensity. High amplitudes or unstable growth and lamellar shape of graphite favour the formation of satellite cracks parallel to the moving main crack by expansion of graphite particles.

The data from the tensile test are summarized in Table III. The non-linearity of the elastic moduli of lamellar cast iron has been confirmed (Fig. 6). It is in accord with the observations of the microstructure under stress (Fig. 5).

An essential part of the experimental investigation are the da/dN (ΔK) curves (Fig. 7). Different critical K-values from static tests have been added into these curves. in Fig. 7a two different melts of the same type of standard cast iron with lamellar graphite have been compared in order to characterize the range of the results. Fig. 7b provides an example for the effect of $R = K_{min}/K_{max}$ on the da/dN (ΔK) curve. As expected, a slight increase in crack growth rate is found for the higher portion of static tension ($R = 0.2$).

Measurements with additional spherulitic graphite irons (Fig. 7c) indicate, that higher tensile strength is not paralleled by better fracture mechanical properties as compared to the irons

TABLE II Quantitative metallography of the alloys (Table I)

Alloy	Vol. fraction (%)			Morphology of graphite	
	Graphite	Pearlite	Ferrite	Diameter (m)	Length (m)
1	13	Rest	0	$< 1 \times 10^{-6}$	1.2×10^{-4}
2	13	Rest	0	$< 1 \times 10^{-6}$	1.2×10^{-4}
3	13	Rest	2	0.3×10^{-4}	–
4	12	Rest	0	0.2×10^{-4}	–

TABLE III Tensile test data of the alloys (see Fig. 2)

Designation of alloys		$R_{P0.2}$ (MPa)	R_m (MPa)	δ_B (%)	HB
1	GG 30 S	200	228	0.5	198
2	GG 30 T	162	188	0.5	177
3	GGG 70 T	356	615	3	234
4	GGG 80 S	469	802	5	260

with lamellar graphite. Spherulitic materials showed a decreasing fracture toughness with increasing tensile strength as is known for many high strength steels.

Examples of force–displacement curves have been selected for Fig. 8. The ΔK-axes of Fig. 7 were used to indicate some of the critical K-values which have been measured in static tension. Their meaning is explained in Table IV. $K_{5\%}$-values are in accord with the ASTM Standards. They have been evaluated with the 5% secant-method (Fig. 3a) for all materials. It is indicated which specimen dimension and the conditions for pre-crack formation do not conform with the standard requirements. The large range between the K_c-values and the critical value measured at the end of fatigue crack growth ΔK_m for the materials with lamellar graphite is remarkable. Differently, all critical K-values of the materials with spherulitic graphite are found in a narrow range.

The measurement of crack growth of very small ΔK-values has been limited to $\Delta a = 10^{-9}$ m per cycle, which was defined as ΔK_{th}. The values found are relatively high as compared with some reported in the literature [7]. The use of ultrasonic vibrations (US) appears to be the appropriate method for a still more sensitive measurement of the threshold stress intensity at which fatigue cracks start to move [13]. Preliminary US-measurements indicate a reasonable compatibility with our threshold values, considering that those measurements have to be done with $R = -1$, i.e. tension–compression [14].

4. Discussion

The aspects of the discussions are two-fold. Firstly, the question must be raised as to which critical fracture mechanical properties are the most appropriate to use in design with cast iron. Secondly, the microstructural origin of the fracture behaviour deserves attention, with the aim to derive quantitative relations between microstructural parameters and bulk fracture mechanical properties (Equation 1).

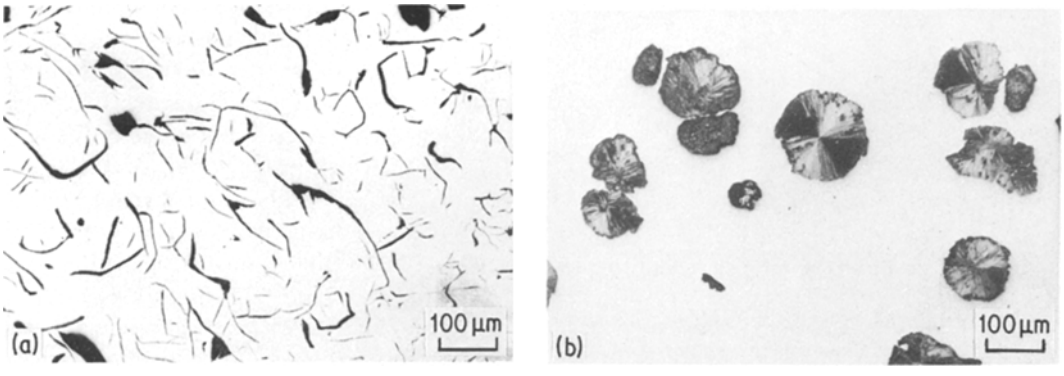

Figure 4 Microstructures of the alloys, unetched. (a) GG 30 (alloy 1), lamellar graphite, (b) GGG 70 (alloy 3), spherulitic graphite.

TABLE IV Fracture mechanical data of the alloys (Figs. 2 and 3 for dimension of specimen and definition of critical K-values)

Alloy		R	ΔK_{th}	ΔK_m	$da/dN = 2.5 \times 10^{-5}$ mm cycle^{-1}			$da/dN = 2.5 \times 10^{-4}$ mm cycle^{-1}		
					K_P	$K_{5\%}$	K_m	K_P	$K_{5\%}$	K_m
1	GG 30 S	0.01	11.5	44.7	–	21.5	32.7	–	26.9	32.8
2	GG 30 T	0.01	12.7	35.3	–	19.2	27.1	–	25.3	28.4
3	GGG 70 T	0.01	16.4	51.5	44.6	43.3	52.3	–	–	–
	GGG 70 T	0.2	16.0	41.3	44.6	43.3	52.2	–	–	–
4	GGG 80 S	0.01	11.0	32.6	31.6	35.4	37.5	32.8	33.7	38.0

The critical K-values permit that stresses can be obtained easily which are useful for the design-engineers. Therefore, K-values were used for the evaluations of the measurements and not crack extension energies (J-integral) [12]. The non-linearity of elastic deformation and the dependence of the elasticity on the amplitude of pre-cycling makes their use problematic for lamellar cast iron. As the stress intensity is raised the following phenomena occur at the crack tip and have effects on the force–displacement curves (Fig. 8):

1. elastic deformation;
2. formation of holes in or at graphite particles;
3. microcrack growth at the edges of these particles;
4. local plastic deformation of the matrix and subsequent pop-in;
5. stable crack growth by microcrack coalescence;
6. instable crack growth through graphite and matrix.

In order to define a reasonable criterion of a critical K-value it should be known which of these crack tip mechanisms can be tolerated (Fig. 3). The flexure of the force–displacement curve may be due to microcracking in an alloy with lamellar graphite, while mainly plastic deformation is found for globular graphite with some soft ferrite as part of the matrix (alloy 3, Fig. 8). Rigid application of the ASTM criteria will lead to results which could be misleading and far underestimate the load carrying ability of lamellar cast iron. Even application of the R-curve concept is not advisable for the alloy with lamellar graphite because of the non-plastic origin of the curvature of the force–displacement curve. To chose stage 4 for the spherulitic and stage 5 for the lamellar cast iron to define an upper level as critical values could provide some comparability between the properties of the two types of material.

Their different behaviour in respect to the conditions under which the pre-crack was produced deserves attention (Fig. 7, Table IV). For iron with spherulitic graphite there exists only a small range between the (ASTM Standard) conditions, $K_{5\%}$, and the value measured when rupture occurred at the end of the $da/dN(\Delta K)$ curve, ΔK_m. Cast iron with lamellar

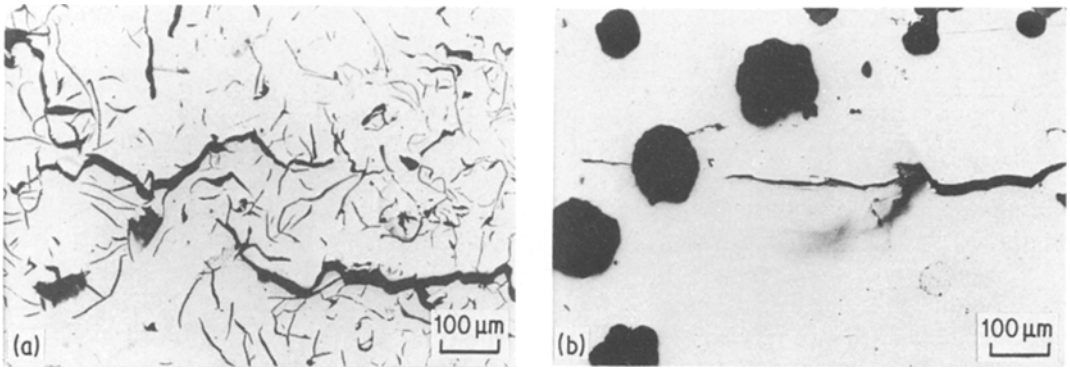

Figure 5 Microstructures at the environment of the crack tip, unetched. (a) GG 30 (alloy 1), crack branching and multiple crack growth, (b) GGG 70 (alloy 3), propagation of an individual crack.

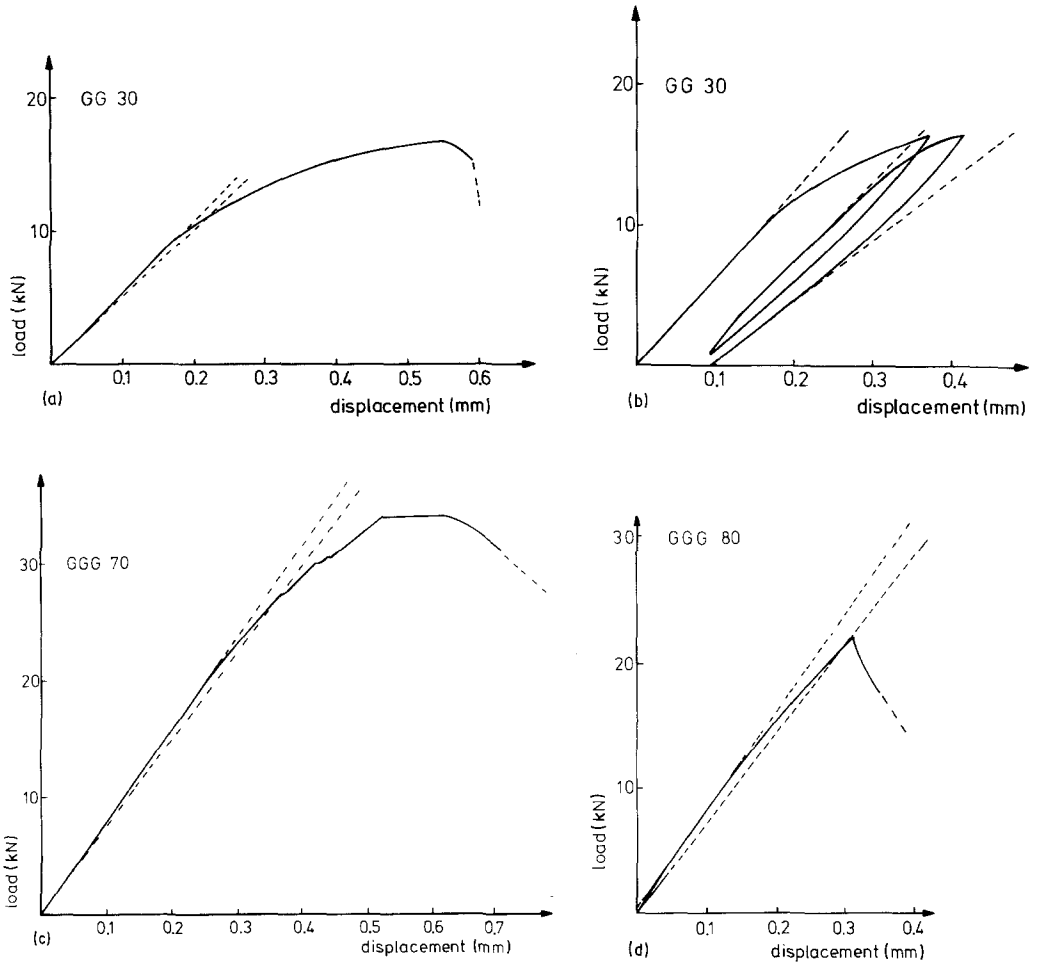

Figure 6 Force–displacement curves for different materials. (a) GG 30 (alloy 1), 5% secant is indicated. (b) GG 30 (alloy 1), two cycles, showing an increased compliance and range of linear elastic behaviour with increasing number of cycles. (c) GGG 70 (alloy 3), 5% secant, pop-in. (d) GGG 80 (alloy 4), 5% secant, coinciding with maximum load.

graphite shows a range with a factor of about 2, between the two values. The high K_{Ic} values given in [6] evidently were ΔK_m-values, i.e. obtained after cycling the pre-crack to the maximum amplitude. With this interpretation these values coincide rather well with the present result. There seem to be no major discrepancies left between different earlier measurements (as claimed by Speidel [7] if the methods of obtaining the critical K-values are taken into consideration. For the practical use of critical K-values in design this means that the $K_{5\%}$-values for lamellar iron underestimate the load carrying ability much more than those of the spherulitic alloy. This is especially true if a critical crack develops by continuous fatigue crack growth. The reason for this behaviour of the lamellar cast iron must be due to fatigue-induced changes in the microstructure: formation and growth of a field of microcracks, cyclic work-hardening of the matrix with increasing amplitude of stress intensity (Fig. 9). Formation and growth of microcracks in a reaction zone is found in martensitic steels [15, 16], as well as in many ceramic materials [17, 18]. It is likely that the extent of crack branching is responsible for the differences which were measured in ΔK_{th} [7] and K_{Ic}.

Using the present observations a refinement of Equation 2 can be proposed. This relation was derived for one unique crack. If crack branching can take place or if satellites accompany the main crack or if the method of precracking has produced a field of microcracks at the tip, additional energy is dissipated. Consequently, a higher stress intensity $K(1 + n)^{1/2}$ is

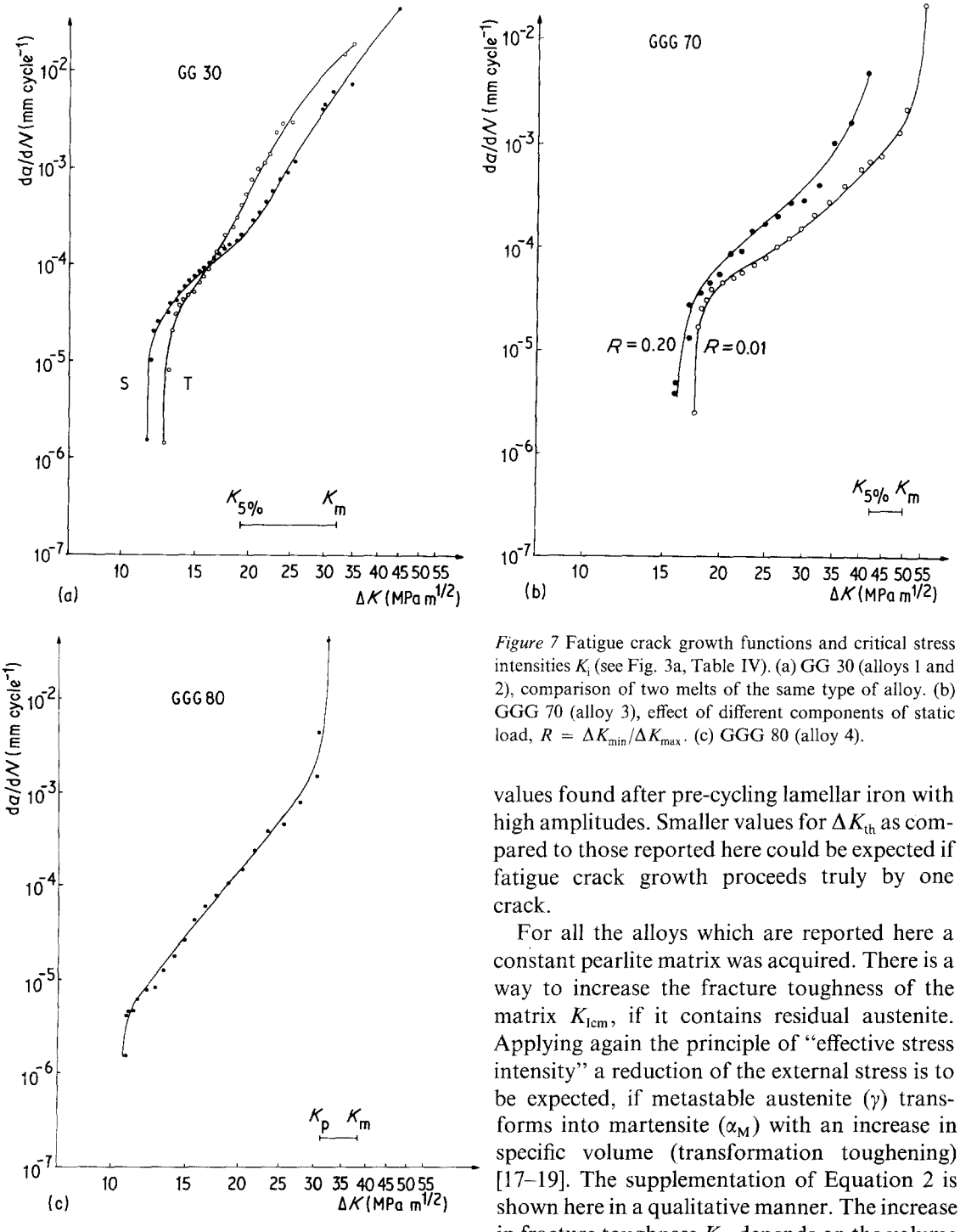

Figure 7 Fatigue crack growth functions and critical stress intensities K_i (see Fig. 3a, Table IV). (a) GG 30 (alloys 1 and 2), comparison of two melts of the same type of alloy. (b) GGG 70 (alloy 3), effect of different components of static load, $R = \Delta K_{min}/\Delta K_{max}$. (c) GGG 80 (alloy 4).

required to propagate the crack. $n > 1$ is the number of cracks that are found parallel to the tip of main crack (Fig. 9):

$$K_{Ic} = \frac{K_{Ic}(1 + n)^{1/2}}{f_m + f_g C[1 + 2(l/\varrho)^{1/2}]} \quad (3)$$

This equation explains the increased critical K-values found after pre-cycling lamellar iron with high amplitudes. Smaller values for ΔK_{th} as compared to those reported here could be expected if fatigue crack growth proceeds truly by one crack.

For all the alloys which are reported here a constant pearlite matrix was acquired. There is a way to increase the fracture toughness of the matrix K_{Icm}, if it contains residual austenite. Applying again the principle of "effective stress intensity" a reduction of the external stress is to be expected, if metastable austenite (γ) transforms into martensite (α_M) with an increase in specific volume (transformation toughening) [17–19]. The supplementation of Equation 2 is shown here in a qualitative manner. The increase in fracture toughness K_{Ct} depends on the volume fraction of residual austenite, the fraction which is actually transformed, and the volume change associated with the transformation in a particular alloy [19].

$$K_{Ic} = \frac{(K_{Icm} + K_{Ct})(1 + n)^{1/2}}{f_m + f_g C[1 + 2(l/\varrho)^{1/2}]} \quad (4)$$

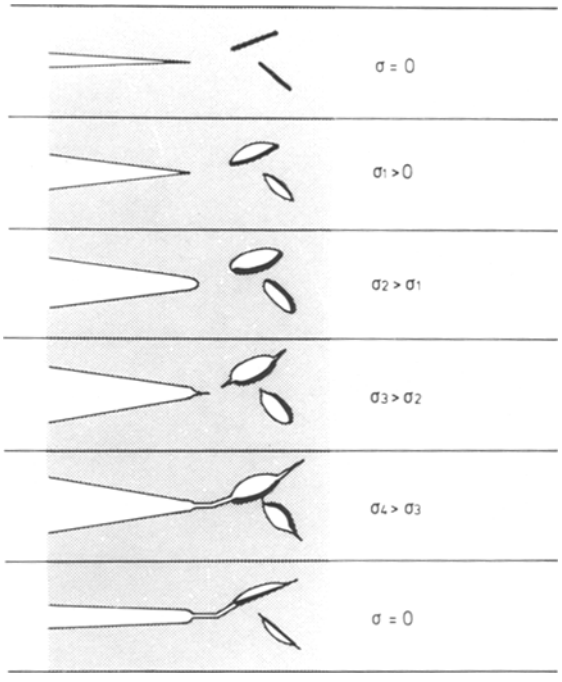

Figure 8 Mechanism of crack growth in cast iron with lamellar graphite. $\sigma = 0$, undeformed structure; σ_1, separation in graphite; σ_2, plastic deformation in matrix (ferrite); $\sigma = 0$, crack progress after removal of load. Schematic drawing.

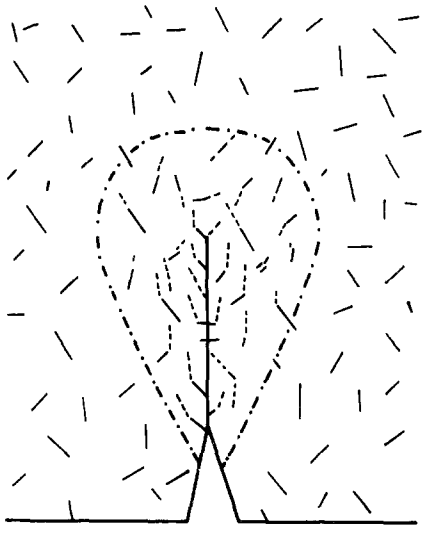

Figure 9 The observed mechanism of crack growth in GG 30: formation of parallel cracks and crack branching. Schematic drawing.

(K_{Icm} + K_{Ct}) is the effective fracture toughness of a matrix containing a metastable phase which is able to transform in the stress field of the crack. It indicates relations between important microstructural parameters and bulk fracture mechanical properties, which may help in designing cast irons with improved properties.

5. Conclusions

1. Cast irons with lamellar and spherulitic graphite show a completely different origin of their load–displacement curves in static fracture mechanical testing.

2. Spherulitic iron behaves, in principle, analogously to steels. Plastic deformation and work-hardening of the metallic matrix takes place during fatigue and precedes rupture.

3. The microstructure of lamellar iron is changed in addition by formation and expansion of microcracks under subcritical static and dynamic loading conditions. Consequently a mechanical pretreatment affects the elastic modulus.

4. In such a structure the critical stress intensity, as determined by a certain flexure of the load–displacement curve, leads to small critical K-values.

5. As a consequence, there is a wide range (factor of 2) between a critical stress intensity determined by the ASTM Standard (5% secant) and the maximum load bearing capacity (ΔK_m) for lamellar iron.

6. Conventionally measured K_{Ic}-values of lamellar cast iron therefore far underestimate the resistance of this material to crack growth in comparison to iron with spherulitic graphite and steel.

7. Simple models have been proposed for the relation between the microstructure of this group of material and fracture toughness, i.e. the stress intensity at which unstable crack extension starts.

8. Microstructural parameters are volume fraction, shape and distribution of graphite, the properties of the metallic matrix, and microcracks (eventually produced by a mechanical pretreatment).

9. Such models could be used for microstructural design. The present relations already explain rather well the order of magnitude of the measured data. A refinement is possible, for example, by considering primary dendritic crystallization, in the as-cast structure, or by the application of new mechanisms such as transformation toughening by residual austenite.

10. Some uncertainty is left about the amount

of the ΔK_{th}-value, i.e. the start of fatigue crack growth. Crack branching and satellite formation at graphite particles make measurements in this range difficult and ambiguous.

Acknowledgements

This work would not have been possible without the knowledge and engagement of Mr K. H. Bowe in the field of mechanical testing including the critical discussion of the evaluation of the measurements. In addition thanks are due to Mr K. Rittner for help in conducting the microscopic studies and Professor K. H. Schwalbe for valuable discussion on the evaluation of fracture mechanical measurements. An investigation of the threshold range is under way supplemented by ultrasonic measurements together with Dr S. Stanzl, Vienna University.

The materials came from two sources: Gebrüder Sulzer AG, Winterthur, Switzerland, and Thyssen Gießerei AG, Mülheim, FRG. I would like to thank these firms and especially Dr D. Schock, Winterthur, Professor J. Motz, Gelsenkirchen, and Dr B. Wolters, Mülheim, for their support of this work with various well specified grey cast irons.

References

1. W. ELBER, in ASTM STP 486 (American Society for Testing and Materials, Philadelphia, 1971) pp. 230–40.
2. E. HORNBOGEN, Proceedings ICSMA 6, Vol. 3, Melbourne (Pergamon Press, Oxford, 1982) pp. 1059–73.
3. E. HORNBOGEN and J. MOTZ, *Gießerei Forsch.* **29** (1977) 115.
4. A. G. GLOVER and B. POLLARD, *J. Iron Steel Inst.* (1971) 138.
5. L. GRÜTER, Dr-Ing. thesis, Ruhr-Universität Bochum (1975)
6. *Idem, Gießerei Forsch.* **29** (1977) 23.
7. M. SPEIDEL, *Z. Werkstofft.* **12** (1981) 387.
8. J. MOTZ and C. BERGNER, *Gießerei Forsch.* **32** (1980) 97.
9. S. R. HOLDSWORTH and G. JOLLEY, *Brit. Foundryman.* **68** (1975) 169.
10. J. MOTZ and J. JUST, *Gießerei Forsch.* **28** (1976) 151.
11. K. H. ZUM GAHR and L. WAGNER, *Arch. Eisenhüttenw.* **50** (1979) 269.
12. ASTM Standards: (a) E 399-80 (K_{Ic}), (b) E 24.08.0.4 (J_{Ic}), (c) E 561-76T (R), (d) E 647-78T (da/dN).
13. E. TSCHEGG and S. STANZL, *Acta Metall.* **29** (1981) 21.
14. S. STANZL and R. MITSCHE, *Wiss. Film* **18** (1977) 22.
15. R. B. BROBST and G. KRAUSS, *Met. Trans.* **5** (1974) 457.
16. F. ERVEN and E. HORNBOGEN, *Härtereitechn. Mitt.* **39** (1984) 55.
17. N. CLAUSSEN, J.STEEL and R. F. RABOT, *Amer. Ceram. Soc.* **56** (1977) 559.
18. N. CLAUSSEN and J. JAHN, *ibid.* **61** (1978) 487.
19. E. HORNBOGEN, *Acta Metall.* **26** (1978) 147.

Received 12 October
and accepted 6 November 1984